# Intervalley plasmons in graphene

T. Tudorovskiy* and S. A. Mikhailov
*Institute of Physics, University of Augsburg, D-86135 Augsburg, Germany*
(Received 11 May 2010; published 24 August 2010)

The spectrum of two-dimensional (2D) plasma waves in graphene has been recently studied in the Dirac fermion model. We take into account the whole dispersion relation for graphene electrons in the tight-binding approximation and the local-field effects in the electrodynamic response. Near the wave vectors close to the corners of the hexagon-shaped Brillouin zone we find low-frequency 2D plasmon modes with a linear spectrum. These "intervalley" plasmon modes are related to the transitions between the two nearest Dirac cones.

DOI: 10.1103/PhysRevB.82.073411 PACS number(s): 73.21.−b, 71.10.−w, 71.45.Gm, 73.43.Lp

Graphene, a recently discovered[1,2] two-dimensional (2D) material consisting of a single layer of carbon atoms has been in the focus of experimental and theoretical research in the past years (see Ref. 3 and references therein). The carbon atoms in graphene form a dense 2D honeycomb lattice, [Fig. 1(a)], with two atoms per elementary cell. The band structure of graphene electrons[4–6] consists of two bands touching each other at six points $\mathbf{k}=\mathbf{K}_i$, $i=1,\ldots,6$ at the corners of the Brillouin zone (BZ), see [Fig. 1(b)]. In the vicinity of $\mathbf{K}_i$ the dispersion surface forms two cones with vertexes at $\mathbf{K}_i$. In the intrinsic graphene at zero temperature the lower (hole) band is fully occupied while the upper (electron) band is empty, and the Fermi level goes through the Dirac points. Using the doping or applying a gate voltage between the graphene layer and a substrate (in a typical experiment the graphene layer lies on a $Si/SiO_2$ substrate) one can shift the chemical potential $\mu$ to the electron or to the hole band and vary the density of electrons and/or holes.

Near the Dirac points the graphene quasiparticles have a linear, quasirelativistic dispersion

$$E_{\mathbf{k}l}^{\mathrm{Dir}} = l\hbar V|\mathbf{k}-\mathbf{K}_i|, \quad |\mathbf{k}-\mathbf{K}_i|a \ll 1. \tag{1}$$

Here $l=+1$ and $-1$ correspond to the electron and hole band, respectively, $V\approx 10^8$ cm/s is the Fermi velocity in graphene and $a=2.46$ Å is the lattice constant, [Fig. 1(a)]. It is the massless energy dispersion of graphene quasiparticles [Eq. (1)] that leads to its amazing physical properties and caused the great interest to this material.

In this Brief Report we address the problem of plasma oscillations in graphene. The plasma waves in graphene have been considered in Refs. 7–11. In these publications the plasmon spectrum has been calculated in the long-wavelength limit $qa \ll 1$ from zeros of the Lindhard dielectric function[12]

$$\epsilon_{\mathrm{Dir}}(\mathbf{q},\omega) = 1 - \frac{2\pi g_v g_s e^2}{q\kappa S}\sum_{\mathbf{k}ll'} \frac{f(E_{\mathbf{k}l}^{\mathrm{Dir}}) - f(E_{\mathbf{k}+\mathbf{q},l'}^{\mathrm{Dir}})}{E_{\mathbf{k}l}^{\mathrm{Dir}} - E_{\mathbf{k}+\mathbf{q},l'}^{\mathrm{Dir}} + \hbar\omega + i0} \times |\langle \mathbf{k}+\mathbf{q},l'|e^{i\mathbf{qr}}|\mathbf{k}l\rangle_{\mathrm{Dir}}|^2, \tag{2}$$

which can be obtained within the self-consistent-field approach[13] or, equivalently, in the random-phase approximation. Here $S$ is the area of the graphene sample, $f(E)$ is the Fermi-Dirac distribution function, $-e$ is the electron charge $(e>0)$, $\mathbf{q}=(q_x,q_y)$ is the wave vector of an electric field in the 2D plane, $q=|\mathbf{q}|$, $g_s=g_v=2$ are the spin and valley degeneracies, and $\kappa$ is the dielectric constant of surrounding medium. The wave functions $|\mathbf{k}l\rangle$ have been found from the Dirac approach, when the system is described (near the Dirac points) by the effective Hamiltonian $H_{\mathrm{Dir}}=V\sigma_\alpha \hat{p}_\alpha$, where $\alpha$ takes the values $x,y$, $\sigma_\alpha$ are Pauli matrixes, and $\hat{p}_\alpha$ is the momentum operator. The sub/superscript "Dir" in Eq. (2)

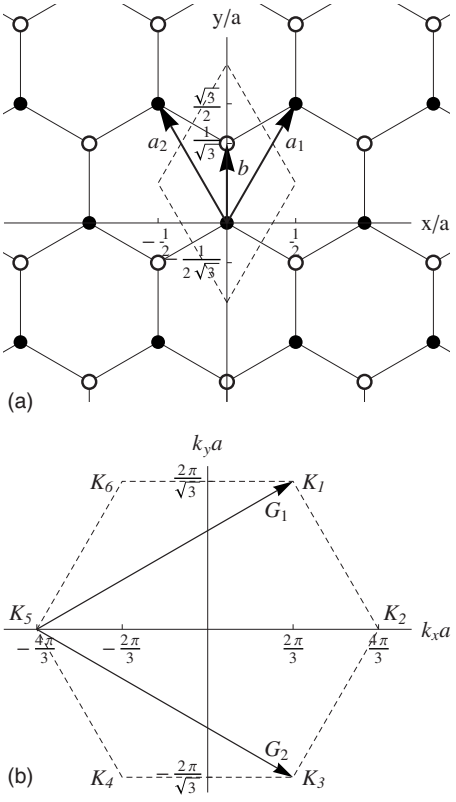


FIG. 1. (a) The honeycomb lattice of graphene. All points of the first sublattice (black circles) are given by $n_1\mathbf{a}_1+n_2\mathbf{a}_2$, of the second sublattice (open circles) by $n_1\mathbf{a}_1+n_2\mathbf{a}_2+\mathbf{b}$. (b) The BZ of graphene. The basis vectors of the reciprocal lattice are $\mathbf{G}_1$ and $\mathbf{G}_2$. The vectors $\mathbf{K}_i$, $i=1,\ldots,6$, correspond to the corners of the BZ (the Dirac points). Dashed lines show the the boundaries of the elementary cell both in direct and reciprocal space. In the figure $\mathbf{a}_1=a(1/2,\sqrt{3}/2)$, $\mathbf{a}_2=a(-1/2,\sqrt{3}/2)$, $\mathbf{b}=a(0,1/\sqrt{3})$, $\mathbf{G}_1=2\pi a^{-1}(1,1/\sqrt{3})$, $\mathbf{G}_2=2\pi a^{-1}(1,-1/\sqrt{3})$, $\mathbf{K}_1=-\mathbf{K}_4=2\pi a^{-1}(1/3,1/\sqrt{3})$, $\mathbf{K}_2=-\mathbf{K}_5=2\pi a^{-1}(2/3,0)$, and $\mathbf{K}_3=-\mathbf{K}_6=2\pi a^{-1}(1/3,-1/\sqrt{3})$, where $a=|\mathbf{a}_1|=|\mathbf{a}_2|$ is the lattice constant and $|\mathbf{G}_1|=|\mathbf{G}_2|=G=4\pi/(\sqrt{3}a)$.

 

reminds that the energies and the wave functions have been calculated within the Dirac (effective medium) approximation. In the limit $q \ll k_F$ the spectrum of 2D plasmons takes the form[7,8]

$$\omega_p(q) = \left(\frac{e^2 g_s g_v |\mu|}{2\hbar^2 \kappa} q\right)^{1/2} = \left(\frac{e^2 V \sqrt{g_s g_v \pi n_s^0}}{\hbar \kappa} q\right)^{1/2}, \quad (3)$$

which coincides with the standard 2D plasmon dispersion $\omega_p(q) = \sqrt{2\pi n_s^0 e^2 q/(m^\star \kappa)}$ with the effective mass being replaced by $m^\star = |\mu|/V^2$. Here $k_F = |\mu|/(\hbar V)$ is the Fermi wave vector and $n_s^0$ is the equilibrium surface density of charge carriers. At $q \gtrsim k_F$ the curve $\omega_p(q)$ enters the region of the interband damping and asymptotically tends to the line $\omega = Vq$.[7–11,14] The 2D plasmons [Eq. (3)] have been experimentally observed in graphene in Refs. 15 and 16.

The results outlined above are based on Eqs. (1) and (2) and are valid in the "long-wavelength" limit, when both the plasmon wave vector $q$ and the Fermi wave vector $k_F$ are small as compared to the reciprocal-lattice vector $G \sim 1/a$. Here we study the 2D plasmon spectrum in graphene at the wave vectors $\mathbf{q}$ close to the corners of the BZ. The 2D plasmons propagate in the same periodic lattice as the 2D electrons and their spectrum $\omega_p(\mathbf{q})$ should be a periodic function of $\mathbf{q}$ with the same hexagon-shaped BZ. Near the corners of the plasmon BZ $\mathbf{q} = \mathbf{K}_i$ one can expect new low-frequency plasmon modes. Indeed, each 2D plasmon wave vector $\mathbf{q} \approx \mathbf{K}_i$ corresponds to an intervalley transition in the electron BZ $\mathbf{K}_j \to \mathbf{K}_{j'}$, for example, $\mathbf{q} = \mathbf{K}_1$ corresponds to the transition $\mathbf{K}_5 \to \mathbf{K}_6$, $\mathbf{q} = \mathbf{K}_2$ to the transition $\mathbf{K}_6 \to \mathbf{K}_1$, and so on. At $\mathbf{q} \approx \mathbf{K}_i$ the energy difference $E_{\mathbf{k}l} - E_{\mathbf{k}'l}$ in the denominator in Eq. (2) is close to zero, which leads to the new, intraband intervalley plasmon modes. In this Brief Report we show that these low-frequency plasmon modes have the linear dispersion

$$\omega_p(\mathbf{q}) = V_p |\mathbf{q} - \mathbf{K}_i|, \quad |\mathbf{q} - \mathbf{K}_i| a \ll 1 \quad (4)$$

with the group velocity $V_p > V$. Figure 2(b) schematically shows the low-frequency plasmon mode in the BZ: the central red square-root "flower" and the blue "flowers" at the corners of the BZ correspond to the conventional intravalley 2D plasmon [Eq. (3)] and the intervalley plasmons, [Eq. (4)] respectively. For comparison, the Dirac cones at the corners of the electronic BZ are shown in Fig. 2(a).

In order to adequately calculate the graphene response at large wave vectors $q \sim 1/a$ one should go beyond Eq. (2) and take into account the local-field effects.[17,18] The electromagnetic response is then described by the matrix dielectric function

$$\epsilon_{\mathbf{G}\mathbf{G}'}(\mathbf{q},\omega) = \delta_{\mathbf{G}\mathbf{G}'} - \frac{2\pi e^2}{\kappa |\mathbf{q}+\mathbf{G}|} \chi_{\mathbf{G}\mathbf{G}'}(\mathbf{q},\omega), \quad (5)$$

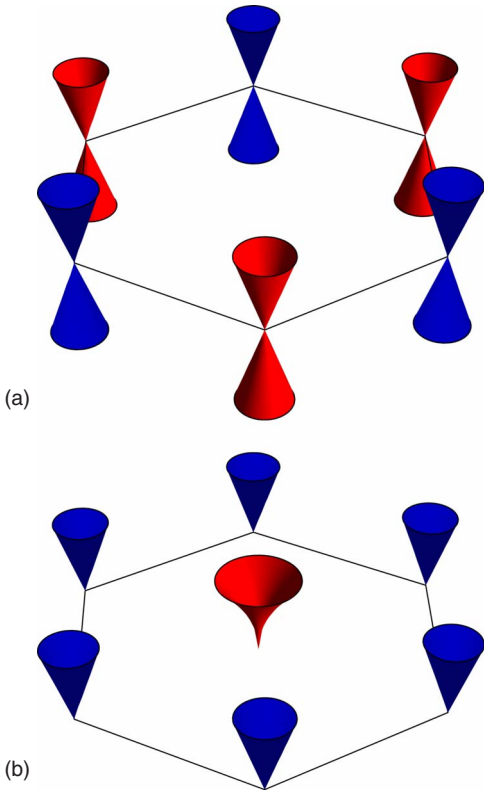


FIG. 2. (Color online) (a) The Dirac cones in the electron BZ and (b) the "flower bed" of the low-frequency 2D plasmon modes in the plasmon BZ.

$$\chi_{\mathbf{G}\mathbf{G}'}(\mathbf{q},\omega) = \frac{g_s}{S} \sum_{\mathbf{k}ll'} \frac{f(E_{\mathbf{k}l}) - f(E_{\mathbf{k}+\mathbf{q},l'})}{E_{\mathbf{k}l} - E_{\mathbf{k}+\mathbf{q},l'} + \hbar\omega + i0} \times \langle \mathbf{k}+\mathbf{q}, l' | e^{i(\mathbf{q}+\mathbf{G}')\mathbf{r}} | \mathbf{k}l \rangle \langle \mathbf{k}l | e^{-i(\mathbf{q}+\mathbf{G})\mathbf{r}} | \mathbf{k}+\mathbf{q}, l' \rangle, \quad (6)$$

where $\mathbf{G}$ and $\mathbf{G}'$ are reciprocal-lattice vectors and $\chi_{\mathbf{G}\mathbf{G}'}$ is the polarizability matrix. The summation over $\mathbf{k}$ in Eq. (5) is performed over the whole BZ, $|\mathbf{k}l\rangle$ are the Bloch functions and $E_{\mathbf{k}l}$ is the corresponding energy dispersion. The 2D plasmon spectrum is determined by zeros of the determinant of $\epsilon_{\mathbf{G}\mathbf{G}'}(\mathbf{q},\omega)$

$$\det \| \epsilon_{\mathbf{G}\mathbf{G}'}(\mathbf{q},\omega) \| = 0. \quad (7)$$

From now on we use the tight-binding approximation[6] for the energy and the wave functions. Then the energy reads $E_{\mathbf{k}l} = l\Delta |\mathcal{S}_{\mathbf{k}}|$, where $\Delta = 2\hbar V/(\sqrt{3}a)$ is the full width of one band and

$$\mathcal{S}_{\mathbf{k}} = 1 + 2e^{i\sqrt{3}k_y a/2} \cos(k_x a/2). \quad (8)$$

The Bloch functions are

$$|\mathbf{k}l\rangle = \frac{1}{\sqrt{2N}} \sum_{\mathbf{a}} e^{i\mathbf{k}\mathbf{a}} [\zeta_{\mathbf{k}}^* \psi(\mathbf{r}-\mathbf{a},z) + l\psi(\mathbf{r}-\mathbf{a}-\mathbf{b},z)], \quad (9)$$

where $N$ is the number of elementary cells inside the area $S$, $\zeta_{\mathbf{k}} = \mathcal{S}_{\mathbf{k}}/|\mathcal{S}_{\mathbf{k}}|$, $\psi$ is the normalized atomic wave function, and $z$ is the perpendicular coordinate. Using the wave functions

[Eq. (9)] one can calculate the matrix elements in Eq. (6)

$$\langle \mathbf{k}l|e^{-i(\mathbf{q}+\mathbf{G})\mathbf{r}}|\mathbf{k}+\mathbf{q},l'\rangle = \frac{1}{2}M(|\mathbf{q}+\mathbf{G}|)[\zeta_{\mathbf{k}}\zeta^{\star}_{\mathbf{k}+\mathbf{q}} + ll'e^{-i(\mathbf{q}+\mathbf{G})\mathbf{b}}], \tag{10}$$

where we assume that $\psi$ depends only on $|\mathbf{r}|$ and $M(q)=\int d^3r|\psi(\mathbf{r},z)|^2e^{i\mathbf{qr}}$. The integration in this formula is performed over the whole three-dimensional space.

If $q \ll 1/a$, the terms $\chi_{\mathbf{GG}'}/|\mathbf{q}+\mathbf{G}| \sim M(\mathbf{q}+\mathbf{G})M(\mathbf{q}+\mathbf{G}')/|\mathbf{q}+\mathbf{G}|$ in [Eq. (5)] are small for all $\mathbf{G}$ and $\mathbf{G}'$ except $\mathbf{G}=\mathbf{G}'=\mathbf{0}$. Then the general 2D plasmon dispersion [Eq. (7)] is reduced to the one used in Refs. 7–11 $\det\|\epsilon_{\mathbf{GG}'}(\mathbf{q},\omega)\| = \epsilon_{\mathbf{00}}(\mathbf{q},\omega)=\epsilon_{\mathrm{Dir}}(\mathbf{q},\omega)=0$. If $\mathbf{q}$ is close to one of the vectors $\mathbf{K}_i$, nine terms in the matrix $\chi_{\mathbf{GG}'}/|\mathbf{q}+\mathbf{G}|$ give a noticeable contribution to the determinant of the matrix $\epsilon_{\mathbf{GG}'}(\mathbf{q},\omega)$. For example, if $\mathbf{q}\simeq\mathbf{K}_5$, the corresponding reciprocal-lattice vectors are $\mathbf{G}=\mathbf{0}$, $\mathbf{G}_1$, and $\mathbf{G}_2$. For them $|\mathbf{q}+\mathbf{G}|\simeq|\mathbf{K}_5|=K$ and the determinant of the infinite matrix $\epsilon_{\mathbf{GG}'}(\mathbf{q},\omega)$ is reduced to the determinant of a $3\times3$ matrix with $\mathbf{G},\mathbf{G}'=\{\mathbf{0},\mathbf{G}_1,\mathbf{G}_2\}$.

In what follows we assume that $\mathbf{q}=\mathbf{K}_5+\tilde{\mathbf{q}}$, $\tilde{q}\ll k_F \ll K$, and the temperature $T=0$. Then one can show that the interband contribution ($l\neq l'$) to the polarizability tensor [Eq. (6)] is negligible and we can use the linear (Dirac) approximation for the energy in the vicinity of both cones. Keeping in [Eq. (6)] only the intraband terms we get the following expression for the polarizability tensor

$$\chi_{\mathbf{GG}'}(\mathbf{q},\omega) = \frac{g_s}{4S}M^2(K)\sum_{\mathbf{k}}\frac{\Theta_{\mathbf{k}}-\Theta_{\mathbf{k}+\mathbf{q}}}{E_{\mathbf{k}+}-E_{\mathbf{k}+\mathbf{q},+}+\mathrm{sgn}(\mu)\hbar\omega} \times \eta_{\mathbf{G}}(\mathbf{k},\mathbf{q})\eta^{*}_{\mathbf{G}'}(\mathbf{k},\mathbf{q}), \tag{11}$$

where $\Theta_{\mathbf{k}}=\Theta(|\mu|-E_{\mathbf{k}+})$, $\Theta$ is the Heaviside step function, $\eta_{\mathbf{G}}(\mathbf{k},\mathbf{q})=\zeta^{*}_{\mathbf{k}+\mathbf{q}}\zeta_{\mathbf{k}}+e^{-i(\mathbf{q}+\mathbf{G})\mathbf{b}}$ and $\mathbf{G},\mathbf{G}'=\{\mathbf{0},\mathbf{G}_1,\mathbf{G}_2\}$; the chemical potential $\mu$ can be both positive and negative, i.e., our results are valid for both electron and hole gases. Then introducing the notations $\mathbf{k}=\mathbf{K}_1+\tilde{\mathbf{k}}$, the angle $\theta_1$ between the vectors $\tilde{\mathbf{q}}$ and $\tilde{\mathbf{k}}$ and the angle $\theta_2$ between the vector $\tilde{\mathbf{q}}$ and $\mathbf{K}_2=-\mathbf{K}_5$, we get

$$\chi_{\mathbf{GG}'} = \frac{3g_s}{4\pi^2\hbar V}M^2(K)\int_0^{k_F}\tilde{k}d\tilde{k}\int_0^{2\pi}d\theta_1 \times \frac{|\tilde{\mathbf{k}}+\tilde{\mathbf{q}}|-\tilde{k}}{-(|\tilde{\mathbf{k}}+\tilde{\mathbf{q}}|-\tilde{k})^2+(\omega/V)^2}f_{\mathbf{G}}(\theta_1+\theta_2)f^{*}_{\mathbf{G}'}(\theta_1+\theta_2), \tag{12}$$

where $f_{\mathbf{G}}(\theta)=(-e^{-2i\theta}+e^{-i\mathbf{Gb}})/\sqrt{6}$ for $\mathbf{G}=\{\mathbf{0},\mathbf{G}_1,\mathbf{G}_2\}$ and $\langle f|f\rangle=\Sigma_{\mathbf{G}=\mathbf{0},\mathbf{G}_1,\mathbf{G}_2}|f_{\mathbf{G}}(\theta)|^2=1$.

If $|\omega|<V\tilde{q}$, the integrand in Eq. (12) has poles on the $\theta_1$ axis and the functions $\chi_{\mathbf{GG}'}$ turn out to be complex. Similar to the standard 2D plasmons[7–11] this corresponds to the single-particle intraband absorption (Landau damping). At larger frequencies, $|\omega|>V\tilde{q}$, the denominator in Eq. (12) does not vanish and the functions $\chi_{\mathbf{GG}'}$ are real. In this region one can therefore expect a weakly damped (at low temperatures) low-frequency plasmon mode. As it will be seen from the result below, the frequency of the new plasmon mode is close to $V\tilde{q}$. Evaluating the leading term of the asymptotics of $\chi_{\mathbf{GG}'}$ with respect to the small parameter $(|\omega|/V\tilde{q}-1)\ll1$ we get

$$\epsilon_{\mathbf{GG}'} \simeq \delta_{\mathbf{GG}'} - \frac{\beta}{\sqrt{|\omega|/V\tilde{q}-1}}f_{\mathbf{G}}(\theta_2)f^{*}_{\mathbf{G}'}(\theta_2), \tag{13}$$

where

$$\beta = \frac{3g_s}{2\sqrt{2}}\frac{e^2}{\hbar V}\frac{k_F}{K}M^2(K). \tag{14}$$

Noticing that the matrix $\epsilon$ can be written as $\epsilon=\mathbb{1}-\mathrm{const}|f\rangle\langle f|$, and using the formula $\det(\mathbb{1}-\mathrm{const}|f\rangle\langle f|) = 1-\mathrm{const}\langle f|f\rangle$ we finally get the spectrum of the intervalley plasmon modes in the form of Eq. (4), where

$$V_p = V(1+\beta^2). \tag{15}$$

As it is seen from Eq. (14) the factor $\beta$ is small as compared to unity.

Calculating the experimentally measurable average Joule heat $\langle Q\rangle=\langle \mathbf{j}^{\star}(\mathbf{r},t)\cdot\mathbf{E}^{tot}(\mathbf{r},t)+\mathrm{c.c.}\rangle/2$ we get

$$\langle Q\rangle = \frac{\kappa\omega K}{2\pi}|\phi_0^{ext}|^2\,\mathrm{Im}[(\epsilon^{-1})_{\mathbf{00}}], \tag{16}$$

i.e., the dynamical structure factor is determined by the imaginary part of the element $\mathbf{G}=\mathbf{G}'=\mathbf{0}$ of the inverted dielectric matrix. The last one is $\mathrm{Im}[(\epsilon^{-1})_{\mathbf{00}}] = (2\pi/3)\beta^2\delta(\omega/V\tilde{q}-1-\beta^2)$.

The intervalley plasmon mode [Eq. (4)] should not be confused with the acoustic plasmons which may exist in two- or multicomponent plasmas and have the linear dispersion $\omega\propto q$ in the long-wavelength limit $q\to0$ (see e.g., Ref. 19, where such low-$q$ plasmon mode has been studied in double-layer graphene). The acoustic modes arise in systems with two (or more) different types of charge carriers, e.g., electrons in different 2D layers, like in Ref. 19, or in different energy subbands in the same layer. In single-layer gated or doped graphene ($|\mu|\gg T$) there exists only one type of charge-carriers electrons in the conduction band or holes in the valence band. The two valleys in graphene describe different quantum states of the same electron but not two different types of electrons. Therefore, in a single-layer graphene there exists only one plasmon mode: in the low-$q$ regime ($q\ll K$) its properties were studied in Refs. 7, 8, and 14, in the high-$q$ limit ($q\simeq K$), at $\mathbf{q}$ close to the corners of the Brillouin zone, it is studied in the present Brief Report. The intervalley plasmon [Eq. (4)] is unique for graphene; it is a direct consequence of the unusual energy dispersion in this material, [Fig. 2(a)]. Notice that the presence of the low-frequency, finite $q$ plasmon mode in graphene may lead to an instability of the system and to formation of the charge-density waves.[20]

In conclusion, we have found the intraband intervalley low-frequency plasmon modes with the linear dispersion [Eq. (4)] and the group velocity [Eq. (15)]. The appropriate description of these modes requires to take into account the local-field effects. The predicted modes do not exist in conventional 2D electron systems and are the unique feature of graphene. They could be observed using Raman or electron energy-loss spectroscopy.[15,16,21–23]

The work was supported by Deutsche Forschungsgemeinschaft and Swedish Research Council.

*Also at Radboud University Nijmegen, Institute for Molecules and Materials, Heyendaalseweg 135, 6525 AJ Nijmegen, The Netherlands; t.tudorovskiy@science.ru.nl

[1] K. S. Novoselov, A. K. Geim, S. V. Morozov, D. Jiang, M. I. Katsnelson, I. V. Grigorieva, S. V. Dubonos, and A. A. Firsov, Nature (London) **438**, 197 (2005).
[2] Y. Zhang, Y.-W. Tan, H. L. Stormer, and P. Kim, Nature (London) **438**, 201 (2005).
[3] A. H. Castro Neto, F. Guinea, N. M. R. Peres, K. S. Novoselov, and A. K. Geim, Rev. Mod. Phys. **81**, 109 (2009).
[4] P. R. Wallace, Phys. Rev. **71**, 622 (1947).
[5] J. C. Slonczewski and P. R. Weiss, Phys. Rev. **109**, 272 (1958).
[6] R. Saito, G. Dresselhaus, and M. S. Dresselhaus, *Physical Properties of Carbon Nanotubes* (Imperial College Press, London, 1998).
[7] E. H. Hwang and S. Das Sarma, Phys. Rev. B **75**, 205418 (2007).
[8] B. Wunsch, T. Stauber, F. Sols, and F. Guinea, New J. Phys. **8**, 318 (2006).
[9] M. Polini, R. Asgari, G. Borghi, Y. Barlas, T. Pereg-Barnea, and A. H. MacDonald, Phys. Rev. B **77**, 081411(R) (2008).
[10] O. Vafek, Phys. Rev. Lett. **97**, 266406 (2006).
[11] A. Hill, S. A. Mikhailov, and K. Ziegler, EPL **87**, 27005 (2009).
[12] J. Lindhard, K. Dan. Vidensk. Selsk. Mat. Fys. Medd. **28**, 8 (1954).
[13] H. Ehrenreich and M. H. Cohen, Phys. Rev. **115**, 786 (1959).
[14] K. W.-K. Shung, Phys. Rev. B **34**, 979 (1986).
[15] Y. Liu, R. F. Willis, K. V. Emtsev, and T. Seyller, Phys. Rev. B **78**, 201403(R) (2008).
[16] T. Langer, J. Baringhaus, H. Pfnür, H. W. Schumacher, and C. Tegenkamp, New J. Phys. **12**, 033017 (2010).
[17] S. L. Adler, Phys. Rev. **126**, 413 (1962).
[18] N. Wiser, Phys. Rev. **129**, 62 (1963).
[19] E. H. Hwang and S. Das Sarma, Phys. Rev. B **80**, 205405 (2009).
[20] G. Grüner, Rev. Mod. Phys. **60**, 1129 (1988).
[21] T. Langer, H. Pfnür, H. W. Schumacher, and C. Tegenkamp, Appl. Phys. Lett. **94**, 112106 (2009).
[22] C. Kramberger *et al.*, Phys. Rev. Lett. **100**, 196803 (2008).
[23] T. Eberlein, U. Bangert, R. R. Nair, R. Jones, M. Gass, A. L. Bleloch, K. S. Novoselov, A. Geim, and P. R. Briddon, Phys. Rev. B **77**, 233406 (2008).